Genetics inMedicine | ORIGINAL RESEARCH ARTICLE

Corrected: Correction

Open

Mitochondrial oxodicarboxylate carrier deficiency is associated with mitochondrial DNA depletion and spinal muscular atrophy–like disease

Veronika Boczonadi, PhD[1], Martin S. King, PhD[2], Anthony C. Smith, PhD[2], Monika Olahova, PhD[3], Boglarka Bansagi, MD[1], Andreas Roos, PhD[1,4], Filmon Eyassu, PhD[2], Christoph Borchers, PhD[5], Venkateswaran Ramesh, MD[6], Hanns Lochmüller, MD[1], Tuomo Polvikoski, MD[7], Roger G. Whittaker, MD[8], Angela Pyle, PhD[1], Helen Griffin, PhD[1], Robert W. Taylor, PhD[3], Patrick F. Chinnery, FRCP, FMedSci[2,9], Alan J. Robinson, PhD[2], Edmund R.S. Kunji, PhD[2] and Rita Horvath, MD, PhD[1]

Purpose: To understand the role of the mitochondrial oxodicarboxylate carrier (SLC25A21) in the development of spinal muscular atrophy-like disease.

Methods: We identified a novel pathogenic variant in a patient by whole-exome sequencing. The pathogenicity of the mutation was studied by transport assays, computer modeling, followed by targeted metabolic testing and *in vitro* studies in human fibroblasts and neurons.

Results: The patient carries a homozygous pathogenic variant c.695A > G; p.(Lys232Arg) in the *SLC25A21* gene, encoding the mitochondrial oxodicarboxylate carrier, and developed spinal muscular atrophy and mitochondrial myopathy. Transport assays show that the mutation renders SLC25A21 dysfunctional and 2-oxoadipate cannot be imported into the mitochondrial matrix. Computer models of central metabolism predicted that impaired transport of oxodicarboxylate disrupts the pathways of lysine and tryptophan degradation, and causes accumulation of 2-oxoadipate, pipecolic acid, and quinolinic acid, which was confirmed in the patient's urine by targeted metabolomics. Exposure to 2-oxoadipate and quinolinic acid decreased the level of mitochondrial complexes in neuronal cells (SH-SY5Y) and induced apoptosis.

Conclusion: Mitochondrial oxodicarboxylate carrier deficiency leads to mitochondrial dysfunction and the accumulation of oxoadipate and quinolinic acid, which in turn cause toxicity in spinal motor neurons leading to spinal muscular atrophy–like disease.

Genet Med advance online publication 8 March 2018

Key Words: metabolite transport; metabolomics; mitochondrial respiratory chain deficiency; neural toxicity; spinal motor atrophy

INTRODUCTION

Several inherited diseases with very variable clinical presentations are associated with dysfunctional mitochondrial carriers (SLC25), which transport nucleotides, keto acids, amino acids, fatty acids, cofactors, and inorganic ions across the mitochondrial inner membrane.[1–5] They cause various metabolic syndromes often affecting skeletal muscle (e.g., rhabdomyolysis, lipid storage myopathy, and neuromuscular transmission), the heart (cardiomyopathy), or the nervous system (e.g., neuropathy, neonatal epileptic encephalopathy, and optic atrophy).[1–3] The heterogeneous clinical presentations of mitochondrial carrier deficiencies may be explained by the wide range of different substrates transported by mitochondrial carriers and their different roles in intermediary metabolism.[1]

SLC25A21 transports 2-oxoadipate and 2-oxoglutarate across the inner membrane of mitochondria by a counter-exchange mechanism.[6] We report a patient who presented with spinal muscular atrophy and mitochondrial myopathy and we show that this is due to a dysfunctional mitochondrial oxodicarboxylate carrier (SLC25A21) caused by a homozygous c.695A > G mutation. Although the p.(Lys232Arg) amino acid change is conservative, we show that the novel pathogenic variant cannot transport substrates, demonstrating a direct functional link. We were able to identify the molecular etiology of the disorder by combining computer modeling of the effect of defective transport on central metabolism, targeted metabolomics, and in vitro studies in human fibroblasts and neuronal cells.

[1]Wellcome Centre for Mitochondrial Research, Institute of Genetic Medicine, Newcastle University, Newcastle upon Tyne, UK; [2]Medical Research Council Mitochondrial Biology Unit, University of Cambridge, Cambridge Biomedical Campus, Cambridge, UK; [3]Wellcome Centre for Mitochondrial Research, Institute of Neuroscience, Newcastle University, Newcastle upon Tyne, UK; [4]Leibniz Institute of Analytic Sciences (ISAS), Dortmund, Germany; [5]UVic-Genome BC Proteomics Centre, Vancouver, British Columbia, Canada; [6]Department of Paediatric Neurology, Royal Victoria Infirmary, Newcastle upon Tyne Foundation Hospitals NHS Trust, Newcastle upon Tyne, UK; [7]Institute for Ageing and Health, Newcastle University, Newcastle upon Tyne, UK; [8]Institute of Neuroscience, Newcastle University, Newcastle upon Tyne, UK; [9]Department of Clinical Neurosciences, University of Cambridge, Cambridge, UK. Correspondence: Edmund R.S. Kunji or Rita Horvath (ek@mrc-mbu.cam.ac.uk or rita.horvath@ncl.ac.uk)
The first two authors contributed equally to this work.
The last two authors contributed equally to this work.

Submitted 30 August 2017; accepted 21 November 2017; advance online publication 8 March 2018. doi:10.1038/gim.2017.251

MATERIALS AND METHODS

Whole-exome sequencing

Exome sequencing was performed on blood DNA using the Illumina Truseq 62-Mb exome capture kit and a HiSeq 2000. Duplicate sequence reads were removed with Fastuniq (v1.1) before alignment against the human University of California–Santa Cruz hg38 reference genome using the Burrows–Wheeler Aligner (v0.7.12). Coding bases had a mean read depth of 69.6-fold and 90.6% of these bases were covered to a minimum read depth of 10-fold. Sequence variants were called using Samtools/Bcftools (v1.3), followed by annotation with Annovar (January 2016 download) and filtering for rare, evolutionarily conserved, predicted damaging, and with known mitochondrial function using custom Perl scripts, and in silico effects were evaluated following the American College of Medical Genetics and Genomics guidelines.[7] The exome pipeline and variant-filtering scripts are available from GitHub (https://github.com/Helgriff/Exome-Pipe). Confirmation of the selected mutations was performed by Sanger sequencing.

Sodium dodecyl sulfate polyacrylamide gel electrophoresis and blue native polyacrylamide gel electrophoresis analysis

For western blotting, whole-cell lysates or mitochondrial extracts isolated from skeletal muscle tissue (50 µg) were separated by sodium dodecyl sulfate polyacrylamide gel electrophoresis (12%). For blue native polyacrylamide gel electrophoresis (BN-PAGE) mitochondria were extracted from control and patient muscle as previously described.[8] The antibodies used are listed in **Supplementary File S1** online.

Transport studies of SLC25A21 expressed in *Lactococcus lactis*

A codon-optimized *SLC25A21* gene was synthesized by GenScript (Piscataway, NJ), and cloned into the expression vector pNZ8048 under the control of a nisin A-inducible promoter.[9] An *N*-terminal truncation of human oxodicarboxylate carrier (Δ2–4) was used to increase transport activity (**Supplementary File S1**, **Supplementary Methods** (for details of *Lactis* growth, liposome and membrane preparations), and **Supplementary Figure S2**).

Transport assays were carried out using a Hamilton MicroLab Star robot (Hamilton Robotics, Birmingham, UK). Transport of [^{14}C]-2-oxoglutarate (American Radiolabeled Chemicals, Saint Louis, MO) was initiated by the addition of 100 µl PIPES buffer (10 mM 1,4-piperazinediethanesulfonic acid, 50 mM NaCl) with 2.5 µM [14C]-2-oxoglutarate (2.04 GBq/mmol) to 5-µg fused membranes in a MultiScreenHTS-HA 96-well filter plate (pore size 0.45 µm; Millipore, Watford, UK). The transport was stopped at 0, 60, 120, 300 s; 10, 15, 20, and 30 min by the addition of 200 µl ice-cold PIPES buffer and filtering using a vacuum manifold, followed by two additional wash steps with 200 µl ice-cold PIPES buffer. Levels of radioactivity in the vesicles were measured by the addition of 200 µl MicroScint-20 (PerkinElmer, Seer Green, UK) and by quantifying the amount of radioactivity (TopCount scintillation counter, PerkinElmer). Initial rates were determined using linear regression.

Computational modeling of SLC25A21 deficiency

Simulations of metabolism during impaired oxodicarboxylate transport were performed by using the MitoCore metabolic model.[10] Several alterations were made to the default model including the incorporation of five additional reactions involved in the production of tryptophan intermediates and the addition of seven "sinks" to allow the efflux of tryptophan and lysine degradation intermediates: quinolinic acid, 2-oxoadipate, kynurenic acid, xanthurenic acid, L-2-aminoadipate, L-pipecolate, and picolinic acid (the adapted model is available upon request). The default uptake parameters of two "fuel" metabolites were altered to prevent their excessive uptake relative to oxygen availability; fatty acids (hexadecanoate) were set at a maximum uptake of 0.4 µmol/min/gDW and the uptake of acetate was prevented. A minimum uptake flux of cytosolic L-lysine and L-tryptophan was set at a rate recorded experimentally for rat heart tissue.[11] As two separate pathways exist to degrade lysine, the reaction for aminoadipate–semialdehyde synthase (ID:R_SACCD3m), part of the saccharopine pathway, was restricted to half of the uptake of lysine. To simulate SLC25A21 dysfunction, the representative transport steps in the model were disabled (IDs: R_2OXOADPTmB_MitoCore, R_2OXOADPTmC_MitoCore, R_2AMADPTmB_MitoCore, and R_2AMADPTmC_MitoCore). Further simulations were performed where the efflux of quinolinic acid and pipecolate were prevented. The system was simulated with Flux Balance Analysis[12] using the objective function of maximum adenosine triphosphate (ATP) production. Simulations were performed in MATLAB (MathWorks, Natick, MA), using the Constraint-Based Reconstruction and Analysis Toolbox[12] (https://opencobra.github.io) and the GNU Linear Programming Kit solver (http://www.gnu.org/software/glpk/).

Metabolite analysis by mass spectrometry

Metabolite measurements were performed by ultrahigh-performance liquid chromatography—tandem mass spectrometry on an Agilent 1290 ultrahigh-performance liquid chromatography system coupled to a Sciex 4000 QTRAP mass spectrometer. For sample preparation, 45 µl of each sample was mixed with 105 µl of acetonitrile. After vortex mixing for 15 s and sonication in an ice-water bath for 1 min, the samples were centrifuged (14,000*g*, 10 min, 4 °C). The supernatants were used for quantitation of the metabolites using two different ultrahigh-performance liquid chromatography–tandem mass spectrometry in multiple reactions monitoring mode methods, as described[13] (**Supplementary File S1**, **Supplementary Methods**).

Cell culture studies

Age-matched control and patient fibroblasts from the Newcastle Biobank were grown in high-glucose Dulbecco's modified Eagle's medium (Sigma, Poole, UK) supplemented with 10% fetal bovine serum and 1% penicillin/streptomycin. SH-SY5Y cells were grown in Dulbecco's modified Eagle's

medium supplemented with 10% fetal bovine serum, 2 mM glutamine, and 1% penicillin/streptomycin. BN-PAGE of the mitochondrial respiratory chain complexes was performed as described previously.[14] For drug toxicity studies growth medium was supplemented with 5 and 50 µM 2-oxoadipic acid (Sigma) and quinolinic acid (Sigma) respectively for 4 days before analysis. Experiments were done in triplicates.

Study of apoptosis in cell cultures with annexin V-FITC/propidium iodide staining

Cell apoptosis was assessed using an Annexin V-FITC/Propidium Iodide Apoptosis Detection Kit (Abcam) (**Supplementary File S1**, **Supplementary Methods**).

Quantification of mitochondrial DNA copy number

Quantification of mitochondrial DNA (mtDNA) copy number was performed using CFX96 Touch Real-Time PCR Detection System (Bio-Rad) in triplicate by duplex TaqMan quantitative polymerase chain reaction amplification of the mitochondrial gene *MTND1* and the nuclear-encoded gene *B2M* as described previously.[15]

RESULTS

Patient

Written consent for the study and photos was provided by the patient and family members, and approved by the local ethics committee (REC 13/YH/0310).

The patient is a 19-year-old daughter (**Figure 1a**) of consanguineous Pakistani parents. She was born at full term with a weight of 3,180 g, had normal early development, and was walking by 15 months. Between age 3 and 5 years her walking deteriorated slowly with frequent falls. At age 5 years her small hand muscles became wasted and clawed, and she developed bilateral foot drop, failure to thrive, and scoliosis.

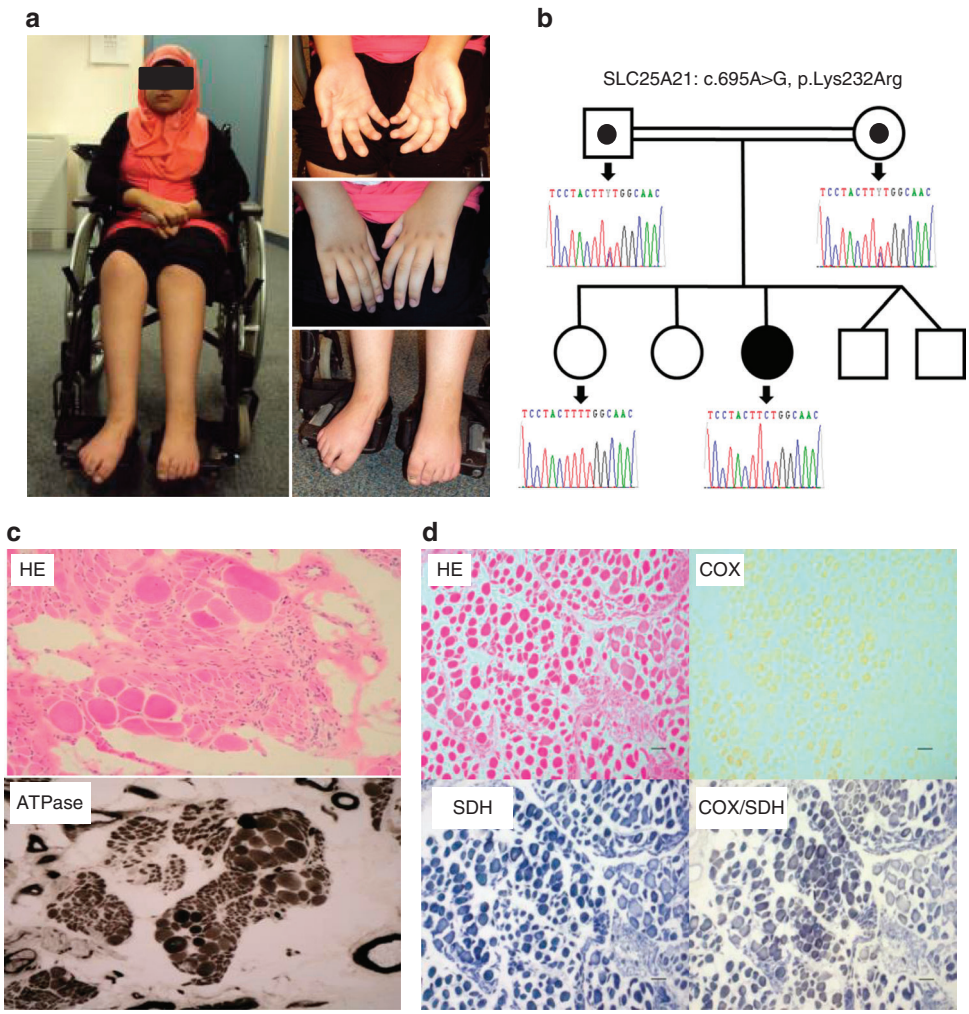

Figure 1 Clinical and laboratory investigations in the patient. (**a**) The patient has a severe distal and proximal weakness affecting the hands and feet and she is wheelchair-bound. (**b**) Sanger sequencing detected the homozygous c.695A > G, p.(Lys232Arg) mutation in the patient, while both parents were heterozygous carriers of this mutation, and the healthy sister was wild type. (**c**) Muscle histology showed some groups of atrophic fibers and groups of hypertrophic fibers, typically seen in spinal muscular atrophy. ATPase pH 4.2 staining demonstrates a significant type grouping, in support of the neurogenic atrophy. (**d**) HE, COX, SDH, COX/SDH. COX is generally weak across the section, also detected in the sequential assay. COX, cytochrome *c* oxidase; HE, hematoxylin and eosin; SDH, succinate dehydrogenase.

On examination, mild facial weakness and tongue fasciculations were noted. Proximal muscle strength was normal, but distal muscle weakness and atrophy in both hands and feet were present. Deep tendon reflexes were brisk in the lower limbs with clonus at the ankles. She was walking with foot drop. Forced vital capacity was 0.74 L (56% of predicted normal value) in a sitting position.

Between 8 and 15 years of age, she deteriorated further with proximal weakness, intermittent relapses triggered by fever, and became wheelchair-bound at age 15. At age 18 she had developed severe weakness (2/5 Medical Research Council grade) resulting in inability to stand with absent deep tendon reflexes. Pulmonary function testing showed forced vital capacity of 65%.

Routine laboratory tests were unremarkable, including renal and liver function, except for a constant microcytic anemia (mean corpuscular volume: 53.9–55.9 fl; hemoglobin 8.6–10.5 g/dl; hematocrit 0.306–0.340%). She had normal levels of creatine kinase, lactate, folate, vitamin E and B_{12}, very-long-chain fatty acids, and phytanic acid. White cell enzymes were normal, including hexoseaminidase and arylsulfatase. Analyses of amino acids in serum and urine showed a slight, but reproducible, increase in lysine, histidine, threonine, serine, glycine, tyrosine, cysteine dimer, alanine, and asparagine. Analyses of the organic acids in urine showed some lactic aciduria and slightly increased excretion of 3-hydroxyisovaleric and glutaric acids. Plasma-free and total carnitine levels were within acceptable ranges. Cerebrospinal fluid was acellular with normal protein and amino acids, but lactate was marginally elevated (2.09 mmol/l versus normal of less than 2 mmol/l). Cranial and spinal magnetic resonance images were unremarkable.

Neurophysiological examination showed severe neurogenic change consistent with an anterior horn cell process. A nerve biopsy suggested an axonopathy, with mild and patchy loss of myelinated fibers. Electron microscopy showed many fibers accumulating membranous and granule debris, and glycogen deposits in the cytoplasm of the Schwann cells (data not shown).

Genetic analysis of the patient's exome

Exome sequencing of the patient's genomic DNA identified three homozygous rare missense variants in *SLC25A21*, *DTNA*, and *HCCS* (minor allele frequency <0.01) that were predicted as "probably damaging" by SIFT, Polyphen-2, LRT, Mutation Taster, FATHMM, PROVEAN, and CADD. Segregation analysis in the patient, both parents, and an unaffected sister showed segregation only with the c.695A > G; p.(Lys232Arg) mutation in *SLC25A21*, encoding the mitochondrial oxodicarboxylate carrier protein (SLC25A21) (**Figure 1b**), which transports 2-oxoadipate into the mitochondrion in exchange for oxoglutarate. This mutation was absent from the ExAC control database (http://exac.broadinstitute.org/), but reported in gnomAD as a heterozygous variant in a single individual from South Asia (http://gnomad.broadinstitute.org/variant/14-37154039-T-C). This region encompasses the patient's Pakistani heritage and suggests she may not be a unique case amongst this population. To identify further undiagnosed cases of mitochondrial oxodicarboxylate carrier deficiency, we searched for patients with a similar phenotype and carrying mutations in the *SLC25A21* gene in various international matchmaking databases, including RD-CONNECT (http://rd-connect.eu/), GeneMatcher (http://genematcher.org), and Matchmaker Exchange (www.matchmakerexchange.org), but we did not identify any other cases suggesting the rarity of this disease. The exome-sequencing data were deposited in the RD-CONNECT database. We studied the effect of this mutation on the expression and function of the SLC25A21 protein.

Skeletal muscle biopsy

A muscle biopsy at 8 years of age suggested neurogenic atrophy with grouping of smaller predominantly type I fibers and increased adipose tissue (**Figure 1c**). Oxidative enzyme histochemistry revealed numerous cytochrome *c* oxidase (COX) deficient fibers (**Figure 1d**) with direct biochemical assay of respiratory chain function revealing decreased activities of complex I (0.026 nmol/UCS (unit of citrate synthase), normal range 0.104 ± 0.036 nmol/UCS) and complex IV ($0.231 \times 10-3$ K.sec^{-1} UCS^{-1}, normal range 1.124 ± 0.511) with normal activities of complexes II and III. A significant decrease in quantitative mtDNA levels ($<10\%$ of age-matched controls) was detected in muscle by reverse-transcription polymerase chain reaction, suggesting mtDNA depletion (**Supplementary File S1**, **Supplementary Figure S3**), although screening of the *TK2*, *RRM2B*, and *POLG* genes encoding proteins involved in mtDNA maintenance failed to detect any candidate pathogenic variants. Her karyotype was normal and deletion of *SMN1* was excluded.

Decreased steady-state levels of multiple respiratory chain complexes in skeletal muscle, but not in fibroblasts

Immunoblotting for mitochondrial proteins in skeletal muscle detected decreased steady-state levels of subunits of complexes I, IV, and V, which was confirmed on BN-PAGE (**Figure 2a–d**). The involvement of complexes I, IV, and V but not complex II suggests a defect involving mtDNA expression or translation, since complex II is the only oxidative phosphorylation complex that does not contain subunits encoded by mtDNA. No significant decrease in the expression of the mitochondrial respiratory chain complexes was detected in fibroblasts. Reduced levels of SLC25A21 were found by immunoblotting in the patient's fibroblasts suggesting that the mutation slightly affects expression or turnover of the protein (**Figure 2e–g**).

The p.(Lys232Arg) variant inactivates the transport function of SLC25A21

Mitochondrial carriers, like SLC25A21, have a single substrate binding site and a cytoplasmic and matrix salt bridge network, which regulates access to the substrate binding site from either side of the membrane.[16] The pathogenic p.(Lys232Arg) variant affects the matrix salt bridge network of the

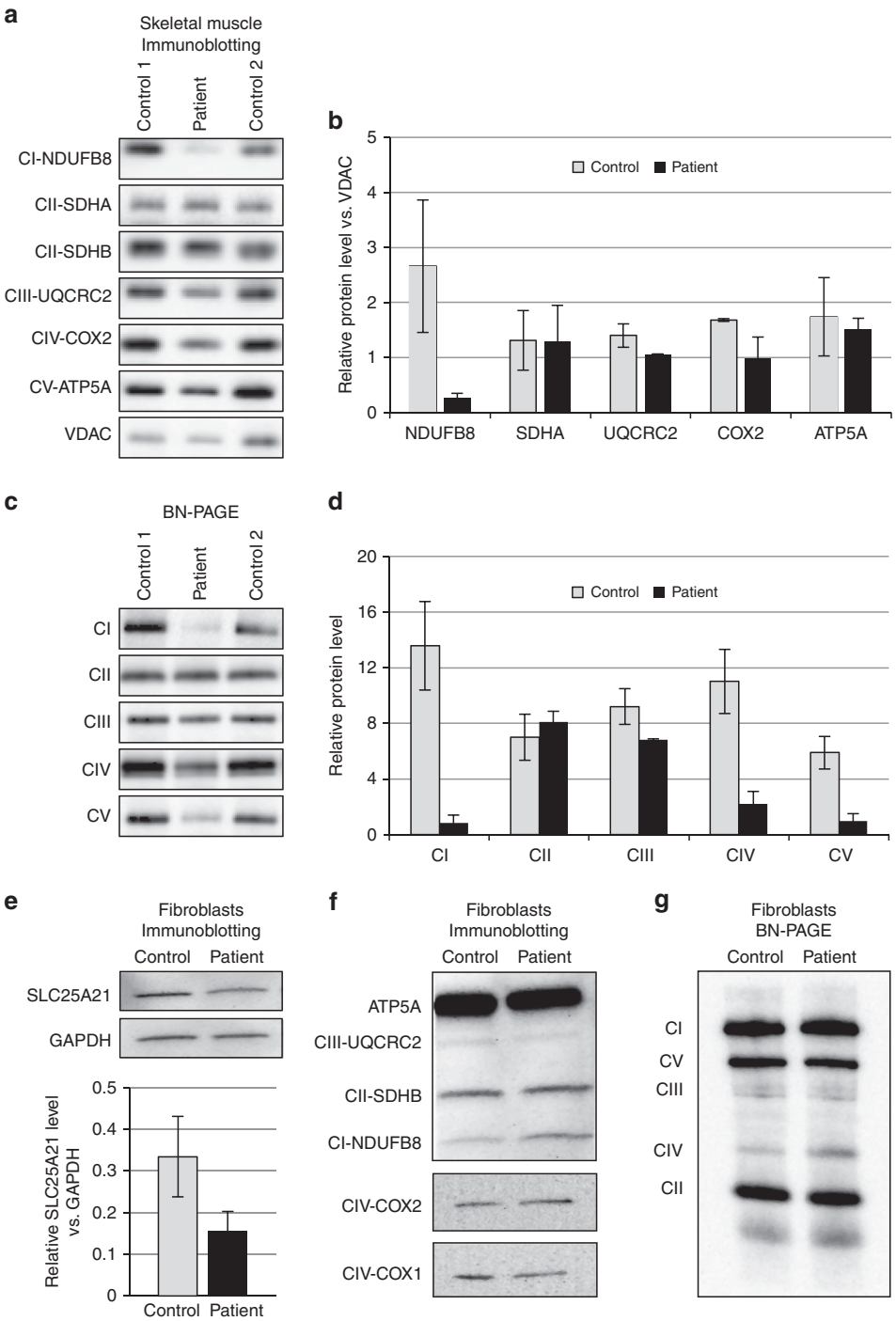

Figure 2 Immunoblotting and blue native polyacrylamide gel electrophoresis (BN-PAGE) in skeletal muscle and fibroblasts. (**a**,**b**) In skeletal muscle immunoblotting detected decreased steady-state levels of mitochondrial oxidative phosphorylation complex subunits for complexes I, III, IV, and V. (**c**,**d**) BN-PAGE detected reduced complexes I, IV, and V. (**e**) Immunoblotting detected slightly reduced SLC25A21 in the patient's fibroblasts, while (**f**) mitochondrial oxidative phosphorylation proteins were normal. (**g**) BN-PAGE detected normal respiratory chain complexes in the patient's cell line. Nuclear-encoded GAPDH, VDAC, SDHA, or SDHB proteins were used as loading controls. ATP5A, F_1F_O adenosine triphosphate synthase subunit; CI, complex I (etc.); CV, complex V/F_1F_O adenosine triphosphate synthase; COX1, cytochrome *c* oxidase 1; COX2, cytochrome *c* oxidase 2; GAPDH, glyceraldehyde 3-phosphate dehydrogenase; NDUFB8, nicotinamide adenine dinucleotide plus hydrogen (NAD) dehydrogenase ubiquinone 1 beta subcomplex subunit 8; SDHA, succinate dehydrogenase subunit A; SDHB, succinate dehydrogenase subunit B; UQCRC2, ubiquinol-cytochrome *c* reductase core protein II; VDAC, voltage-dependent anion-selective channel.

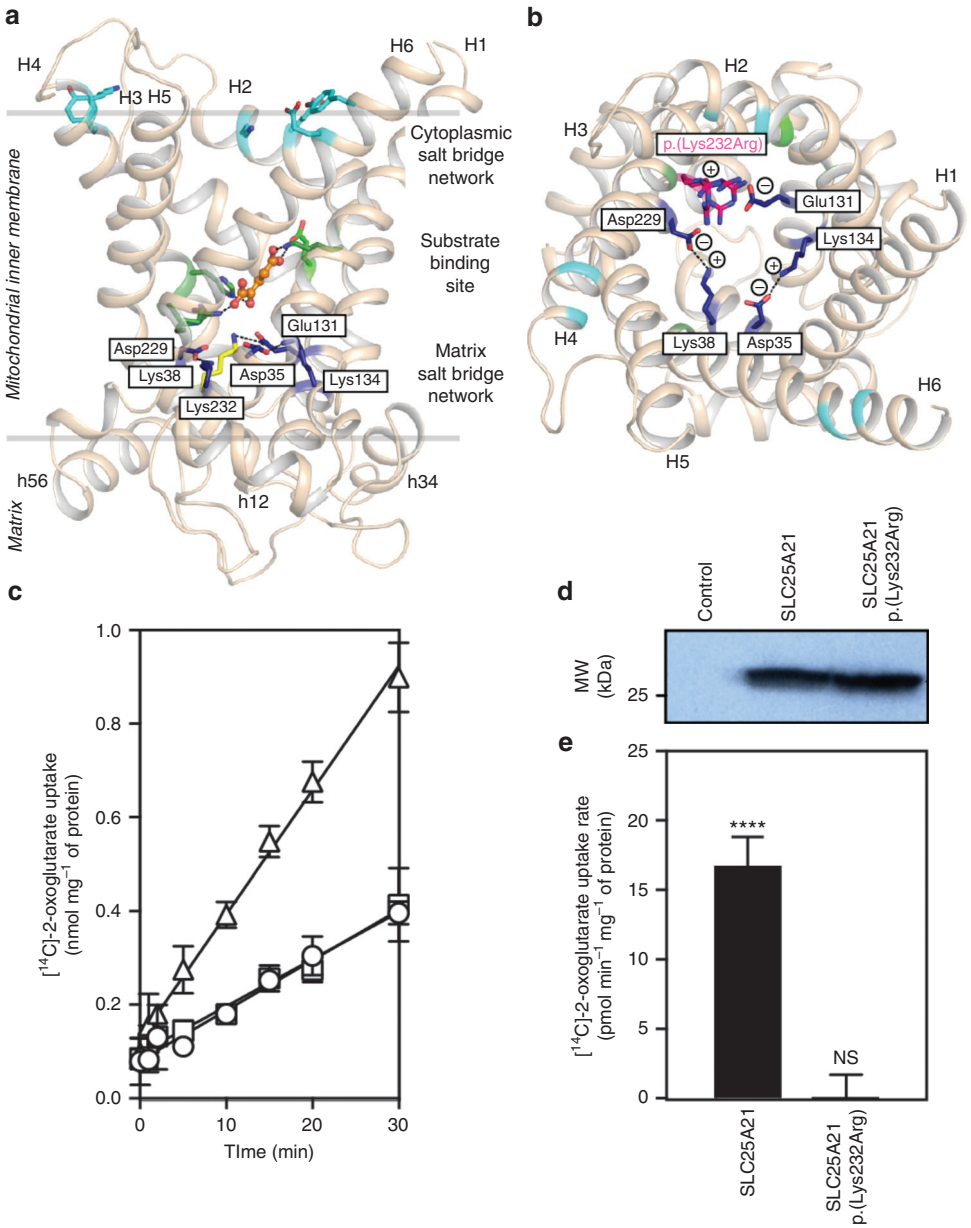

Figure 3 The p.(Lys232Arg) mutation interferes with the formation of the matrix salt bridge network and impairs function of the mitochondrial oxodicarboxylate carrier (SLC25A21). (**a**) Membrane view of the comparative homology model of human SLC25A21 generated with SwissModel (Arnold et al.,[41]) based on the structure of the bovine adenosine diphosphate/adenosine triphosphate carrier (alignment shown in **Supplementary File S1**, **Supplementary Figure S1**). The matrix and cytoplasmic salt bridge network are shown in dark blue and cyan, respectively. The mutated lysine 232 is shown in yellow. The residues of the proposed substrate binding site are shown in green and the substrate 2-oxoglutarate is shown in an orange ball and stick representation. (**b**) Cytoplasmic view showing the residues involved in the formation of the matrix salt bridge network in dark blue. The most probable side-chain conformations of the p.(Lys232Arg) mutation are shown in magenta, indicating that the substitution might impair binding to Glu131 and might lead to other polar interactions. (**c**) The 2-oxoglutarate uptake curves of SLC25A21 and SLC25A21_p.(Lys232Arg). Fused membrane vesicles of *Lactococcus lactis* expressing SLC25A21 (triangles) or SLC25A21_p.(Lys232Arg) (circles) were preloaded with 5 mM 2-oxoglutarate and transport was initiated with the external addition of 1.5 μM [^{14}C]-2-oxoglutarate. Membranes of the uninduced SLC25A21 strain (squares) show background binding, indicating that SLC25A21_p.(Lys232Arg) does not transport above background. (**d**) Expression levels of the wild-type and mutant SLC25A21 were similar, indicating the mutation did not affect expression and insertion of the carrier in lactococcal membranes. (**e**) The 2-oxoglutarate transport rates of SLC25A21 and SLC25A21_p.(Lys232Arg) after correction for background binding. The error bars represent the standard deviation of four technical repeats. Student t-tests, significant uptake above background: $P > 0.05$, not significant (NS); *$P < 0.01$; **$P < 0.001$; ***$P < 0.0001$; ****$P < 0.0001$.

SLC25A21, as Lys232 is predicted to form a salt bridge interaction with Glu130 of the neighboring domain (**Figure 3a**). Although the predicted amino acid substitution is conservative, it may prevent the interaction or cause other interactions that may ablate the function of the protein (**Figure 3b**). To study the effect of the genetic variant on transport of 2-oxoglutarate, truncated versions of the human wild-type and disease variant p.(Lys232Arg) were expressed in the cytoplasmic membrane of *Lactococcus lactis* under control of the Nisin A promoter.[17] Expression levels of the wild-type and the p.(Lys232Arg) variant were similar, indicating the mutation does not affect expression and insertion of the carrier in lactococcal membranes (**Figure 3d**). Wild-type SLC25A21 transported 2-oxoglutarate at a similar rate as the orthologous yeast ODC1 and ODC2 as measured by the uptake of [^{14}C]-labeled 2-oxoglutarate into fused membrane

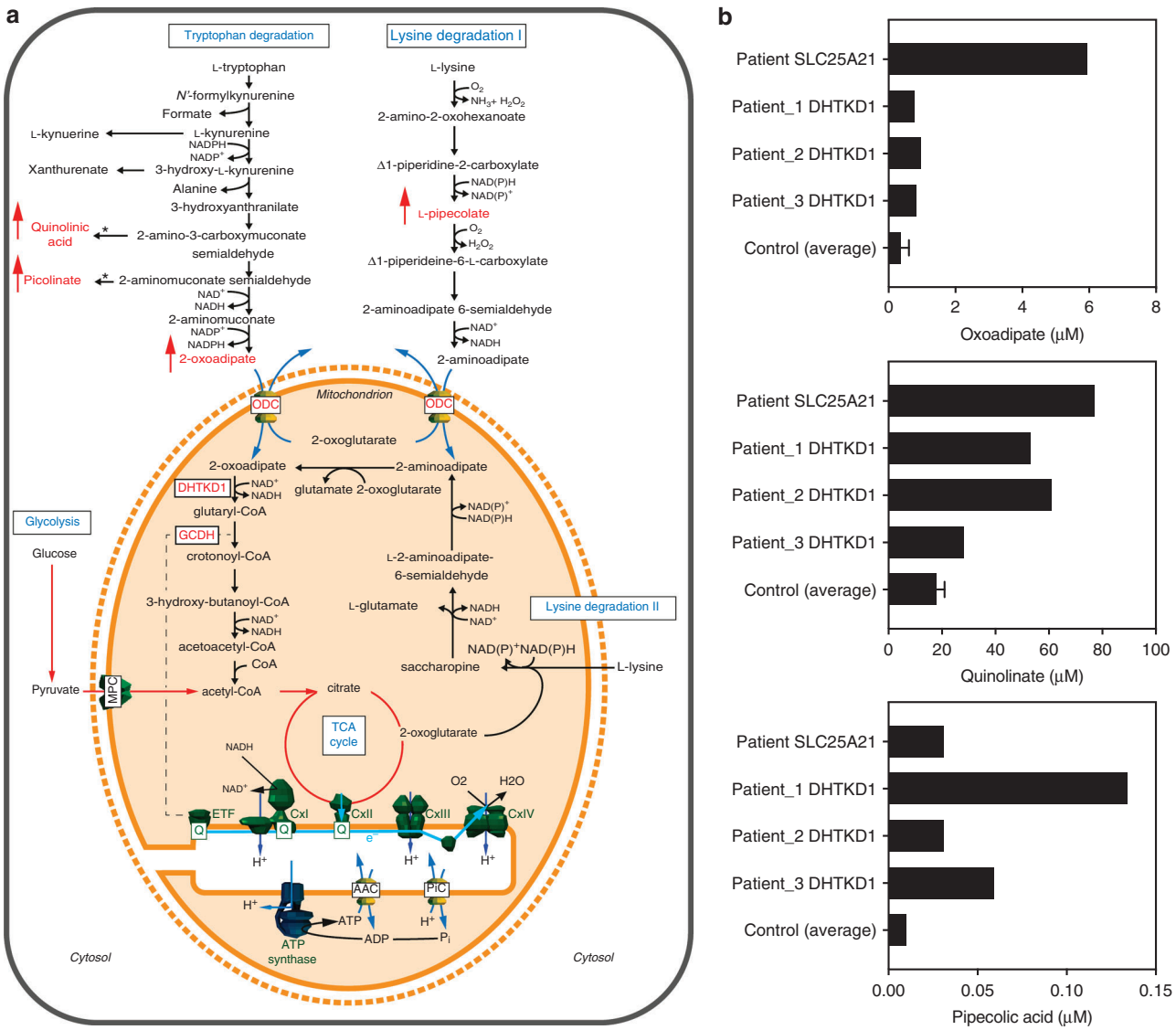

Figure 4 Metabolism of tryptophan and lysine is impaired by mitochondrial oxodicarboxylate carrier deficiency. (**a**) The degradation pathways of tryptophan and lysine run through the mitochondrion, which links it to the generation of adenosine triphosphate through the production of nicotinamide adenine dinucleotide plus hydrogen (NADH), which leads to the reduction of the co-enzyme Q (Q) via complex I, the production of acetyl-CoA, which enters the tricarboxylic acid (TCA) cycle, and through the reduction of the Q pool directly via glutaryl-CoA dehydrogenase and the electron-transferring flavoprotein (dashed line). The metabolic model predicts an increase in quinolinic acid and picolinate levels, which are spontaneously (*) formed from semialdehydes, and in oxoadipate and pipecolate levels, because the import of 2-oxoadipate and 2-aminoadipate into mitochondria is blocked by mitochondrial oxodicarboxylate carrier deficiency (red arrows). These intermediates may have neurotoxic effects, leading to neuropathy. (**b**) Targeted metabolic analysis detected increased 2-oxoadipate, quinolinic acid, and pipecolic acid in the patient and in three other patients carrying *DHTKD1* mutations. ADP, adenosine diphosphate; ATP, adenosine triphosphate; CxI, complex I (etc.); ETF, electron transfer flavoprotein; GCDH, glutaryl-CoA dehydrogenase; ODC, oxodicarboxylate carrier; AAC, ADP/ATP carrier; PiC, phosphate carrier; MPC, mitochondrial pyruvate carrier; Q, ubiquinone..

vesicles in exchange for incorporated unlabeled substrate.[18] In contrast, the p.(Lys232Arg) variant of SLC25A21 did not transport 2-oxoglutarate above background levels, indicating that the function of the transport protein was completely impaired (**Figure 3c**). This is consistent with the equivalent mutation in the bovine mitochondrial oxoglutarate carrier,

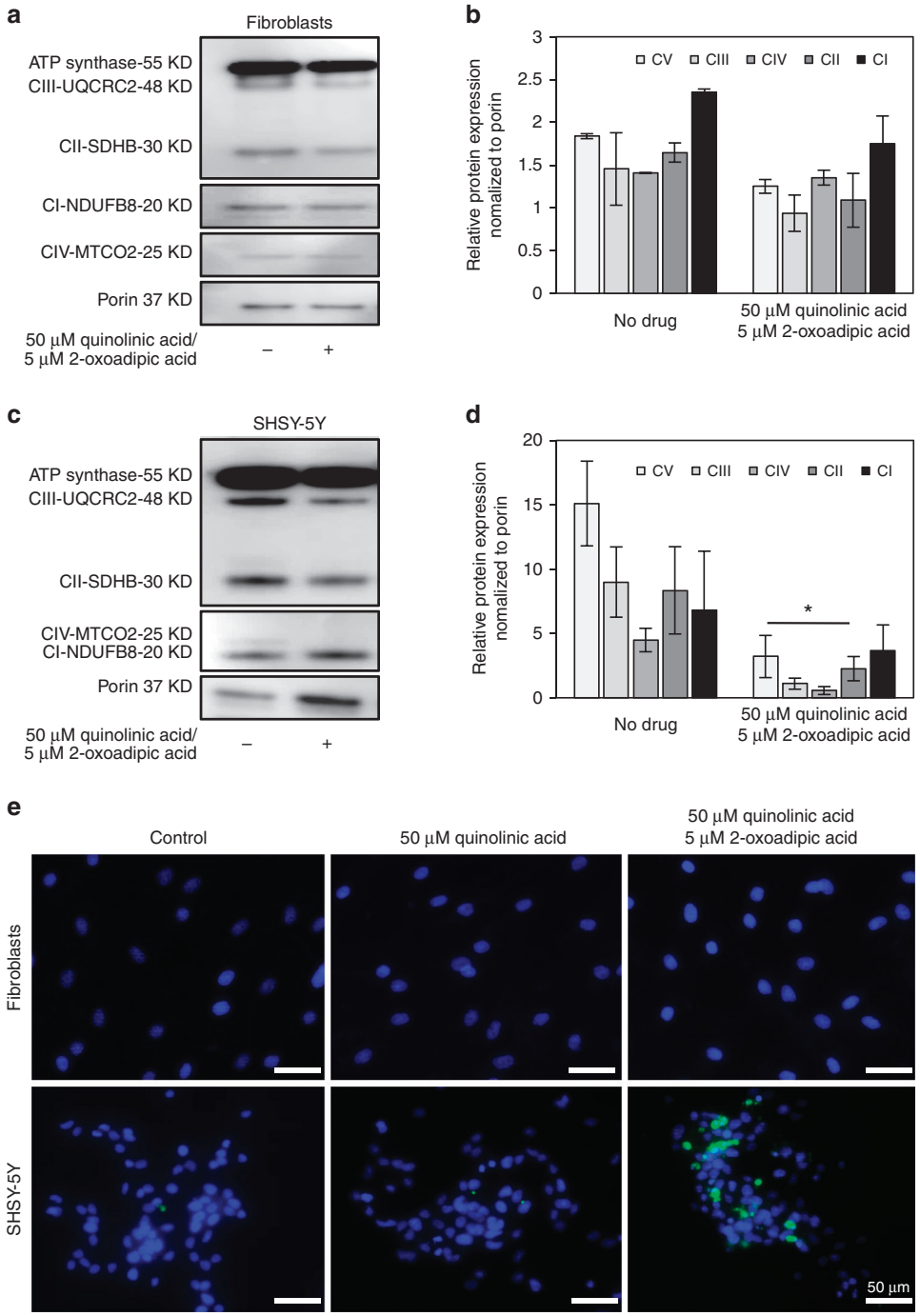

Figure 5 Administration of 2-oxoadipate and quinolinic acid in vitro was more toxic for neuronal cells than fibroblasts. (**a**) Western blot analysis detected normal expression in control fibroblasts after supplementation of 50 μM quinolinic acid and 5 μM 2-oxoadipate after 4 days. (**b**) Quantification of protein levels were normalized to porin. (**c**) In human neuroblastoma cells (SHSY-5Y) the supplementation of the 50 μM quinolinic acid and 5 μM 2-oxoadipate resulted in significantly reduced levels affecting all five oxidative phosphorylation complexes, as shown in (**d**) (n = 3 experimental replicates). P values are from one-way analysis of variance test. Where indicated $*P < 0.05$. (**e**) Visualization of apoptotic cells stained with annexin V-FITC using confocal microscopy after treatment with only 50 μM quinolinic acid and combination of 50 μM quinolinic acid and 5 μM 2-oxoadipate. Cells were supplemented for 4 days before staining. DAPI staining was used as nuclear marker. Top row shows fibroblasts where no annexin V–positive cells were detected in any treatment. Bottom row shows SHSY-5Y cells: Indication annexin V–positive cells were identified after double supplementation. Scale bar = 50 μM. ATP, adenosine triphosphate; CI, complex I (etc.); CV, complex V/F_1F_O adenosine triphosphate synthase; COX1, cytochrome *c* oxidase 1.

p.(Lys244Arg), which also showed no discernible uptake above background.[18] The matrix salt bridge network is a highly conserved feature of mitochondrial carriers and is critical for their function. Thus, we conclude that the p.(Lys232Arg) variant causes SLC25A21 deficiency.

Computational modeling of mitochondrial oxodicarboxylate carrier (SLC25A21) deficiency predicts build-up of degradation intermediates

To investigate the consequences of impaired oxodicarboxylate transport by SLC25A21, we simulated its effects using the MitoCore computer model of central metabolism.[10] The model provides comprehensive coverage of central metabolism, including pathways for the degradation of lysine and tryptophan. SLC25A21 is modeled as four separate transport steps to reflect its characterized substrate specificity (2-oxoadipate for oxoglutarate, L-2-aminoadipate for oxoglutarate) and forward and reverse directions.[6] We altered the model to allow the production and efflux of various lysine and tryptophan intermediates by including additional reactions and "sinks." First, the model was simulated to maximize ATP production using a mixture of "fuel" metabolites such as glucose, lactate, fatty acids, and a forced minimum uptake of L-lysine and L-tryptophan approximated from physiological measurements taken from rat heart tissue. The mitochondrial oxodicarboxylate carrier deficiency was then simulated by disabling the corresponding transport steps in the model. These simulations showed that although ATP production and respiratory chain fluxes were maintained, there was an increased accumulation of L-pipecolic acid and quinolinic acid, which are intermediates of tryptophan and lysine degradation (**Figure 4a**). However, accumulation of other intermediates, such as L-kynuerine, xanthurenate, picolinate, L-2-aminoadipate, and 2-oxoadipate, was not observed. To identify alternative metabolites, the efflux of L-pipecolic acid and quinolinic acid were disabled in separate simulations. These simulations identified the efflux of 2-oxoadipate as a plausible alternative, as it had no impact on ATP production or central metabolism in general.

Metabolic analysis detects increased levels of oxoadipate, quinolinic acid, and pipecolic acid

Mass spectrometry–based analysis of urine samples derived from the mitochondrial oxodicarboxylate carrier–deficient patient compared with unrelated controls showed increased 2-oxoadipate, quinolinic acid, and pipecolic acid levels in urine samples, as predicted by the metabolic modeling (**Figure 4b**). For comparison, we also studied three additional patients with distal spinal muscular atrophy who carried a mutation in dehydrogenase E1 and transketolase domain containing 1 (*DHTKD1*). DHTKD1 is upstream from SLC25A21 in the tryptophan and lysine amino acid degradation pathways (**Figure 4a**),[19] and, when dysfunctional, may cause similar metabolic changes. The observed elevation of oxoadipate, quinolinic acid, and pipecolic acid levels in all of the patients supports the hypothesis that increases in these metabolites may contribute to spinal motor neuron abnormalities (**Figure 4b**).

Increased levels of oxoadipate and quinolinic acid selectively impair neurons

We supplemented control fibroblasts and neuronal cells (SH-SY5Y) with oxoadipate and quinolinic acid in concentrations similar to the levels detected in the patients. There was no significant defect observed in fibroblasts, but a significant decrease of mitochondrial respiratory chain complexes was noted in neuronal cells on combined oxoadipate and quinolinic acid administration, suggesting a toxic effect of these metabolites for neurons (**Figure 5a–d**). In the treated neuronal cells mtDNA copy numbers showed a slight but significant (<0.05) reduction (**Supplementary File S1**, **Supplementary Figure S4**). Visualization of apoptotic cells stained with annexin V-FITC using confocal microscopy after 4 days of treatment with 50 μM quinolinic acid and 5 μM 2-oxoadipate showed apoptosis in SHSY-5Y cells, while no apoptotic cells were detected in fibroblasts (**Figure 5e**).

DISCUSSION

We report a patient with a novel mitochondrial disease affecting predominantly the spinal motor neurons and skeletal muscle due to dysfunction of the mitochondrial oxodicarboxylate carrier (SLC25A21). Interestingly, a 14q13.3 deletion involving the *SLC25A21* gene has been reported with familial synpolydactyly.[20] However, this was suggested to occur due to the deletion of regulatory elements of the neighboring developmental genes *PAX9* and *MIPOLI*, which occur within introns of the *SLC25A21* gene. Our patient did not have synpolydactyly, probably because the *PAX9* and *MIPOLI* regulatory elements are unaffected. The patient presented with a wide range of metabolic and tissue-specific mitochondrial abnormalities, including mitochondrial respiratory chain deficiencies involving complexes I and IV, associated mtDNA depletion, and metabolic abnormalities. Pathogenic variants in another mitochondrial carrier, *SLC25A4*, that most likely affect the substrate binding and mechanics of the carrier, presented also with severe mtDNA depletion, which was explained by a deficiency of adenosine diphosphate/ATP transport.[21] However, in contrast to mutations in *SLC25A4*, the oxodicarboxylate carrier is not directly involved in mitochondrial nucleotide transport.

The disease is caused by the homozygous p.(Lys232Arg) mutation, which affects the highly conserved matrix salt bridge network motif PX[DE]XX[RK] and impairs oxodicarboxylate transport.[18] An equivalent mutation in the mitochondrial oxoglutarate carrier (p.Lys244Arg) also leads to a dysfunctional protein.[18] Mitochondrial carriers cycle between a matrix and cytoplasmic state, and the matrix network closes the carrier to the mitochondrial matrix, when the carrier is in the cytoplasmic state.[22] Although the arginine substitution will conserve the positive charge, it could impair network formation by changing the salt bridge geometry or by introducing additional polar interactions. We propose that

the mutation causes mitochondrial oxodicarboxylate carrier deficiency because transport is completely abolished, leading to several metabolic abnormalities, which are causative for the severe, tissue-specific defect of mitochondrial respiratory chain enzymes and result in tissue-specific mtDNA depletion. However, we cannot exclude the possibility that the variant was not the sole cause of the phenotype.[23]

To investigate the consequences of mitochondrial oxodicarboxylate carrier deficiency on metabolism, we simulated its effects using the MitoCore computer model of central metabolism.[10] The simulations predicted that three metabolites would accumulate: 2-oxoadipate, L-pipecolic acid, and quinolinic acid. Targeted metabolic analysis by mass spectroscopy confirmed the modeling results by showing an increase in the levels of these metabolites in the patient's urine. To corroborate a pathogenic role for these amino acid degradation intermediates in spinal motor neurons, we performed metabolic testing in three previously reported[19] patients who carried a pathogenic variant in the gene for dehydrogenase E1 and transketolase domain containing 1 (*DHTKD1*) gene, an enzyme that is part of both lysine and tryptophan degradation pathways, and catalyzes the decarboxylation of 2-oxoadipate to glutaryl-CoA. Mutations in *DHTKD1* can be asymptomatic or cause 2-aminoadipic 2-oxoadipic aciduria, resulting in symptoms including mild to severe neurological phenotypes, such as muscular hypotonia, or autosomal dominant peripheral neuropathy,[24,25] and decreased mtDNA copy number, which could be due to reduced mitochondrial biogenesis.[26] However, *DHTKD1* dysfunction as a cause of inherited peripheral neuropathy is still debated due to these heterogeneous clinical presentations. Our results show that the levels of all three metabolites were elevated, which is consistent with literature reports of patients with DHTKD1 deficiency.[24] The lower levels of 2-oxoadipate seen in the urine of these patients compared with SLC25A21 deficiency are presumably due to the transport of 2-oxoadipate into the mitochondrial matrix where it cannot be excreted.

Pipecolic acid levels are increased in several related peroxisome disorders, including Zellweger syndrome,[27] infantile Refsum disease,[28] and neonatal adrenoleukodystrophy,[29] as well as the lysine degradation disorder hyperlysinemia type I,[30] caused by α-aminoadipate semialdehyde synthase deficiency. Zellweger syndrome presents with neurological dysfunction, craniofacial abnormalities, and liver dysfunction;[31] infantile Refsum disease presents with retinitis pigmentosa, peripheral neuropathy, and cerebellar ataxia;[28] and neonatal adrenoleukodystrophy presents with hypotonia and convulsions,[29] whereas hyperlysinemia presents with seizures and mildly delayed psychomotor development.[30] Despite these disorders sharing a common phenotype of neurological dysfunction, it has been suggested that in Zellweger syndrome raised pipecolic acid levels are not the direct cause of pathology but arise as a benign consequence[31] and cases of hyperlysinemia type I have been reported to be asymptomatic.[32]

Quinolinic acid is a precursor for NAD^+ (nicotinamide adenine dinucleotide) biosynthesis,[33–35] and so may have contributed to some of the patient's mitochondrial abnormalities due to a NAD^+ deficiency. It is also a potent neurotoxin with high tendency to form free radicals, and is involved in several neuroinflammatory disorders.[36,37] Quinolinic acid at elevated concentrations causes DNA damage, NAD^+ depletion, increased nitric oxide formation, and cell death in neurons and astrocytes.[33] Quinolinic acid exerts its cytotoxicity[37] by causing overstimulation of the *N*-methyl-D-aspartate receptor, which through free radicals leads to irreversible inhibition of complex I, complex II, ATP synthase, aconitase, creatine kinase, and superoxide dismutase, and mitochondrial DNA damage.[38] In addition, quinolinic acid forms a complex with Fe^{2+} (refs. 32–34) that may result in iron sequestration and probably resulted in the microcytic anemia in the SLC25A21-deficient patient. Quinolinic acid also depletes glutathione in astrocytes via peroxynitrite, causing significant decreases in activity of complexes I and II,[39] which is consistent with the biochemical tests on our patient's respiratory complexes. The presence of elevated lactate levels in the cerebrospinal fluid of the patient may be related to the mitochondrial enzyme defect, but may also be consistent with the increased lactate dehydrogenase activity seen with quinolinic acid neurotoxicity.[33,34,36–39]

Lastly, we tested the effect of quinolinic acid and 2-oxoadipate on neuronal cells and fibroblasts. There was a significant decrease of mitochondrial respiratory chain complexes in neuronal cells, but not fibroblasts, whereas apoptotic cells were only seen with a combination of the two metabolites in neuronal cells. We also detected a significant decrease in mtDNA copy number in the treated neurons (**Supplementary File S1**, **Supplementary Figure S4**). In HepG2 cells with DHTKD1 silenced, a decrease in mtDNA copy number was reported and ascribed to reduced mitochondrial biogenesis.[26] Given that DHTKD1 and SLC25A21 are part of the same pathway, they may share common disease mechanisms, e.g., due to quinolate accumulation. Another example of a metabolic defect in the tricarboxylic acid cycle associated with low mtDNA copy numbers is mutations in *SUCLA2* resulting in mitochondrial encephalomyopathy and mtDNA depletion.

Our data suggest that 2-oxoadipate and quinolinic acid are selectively toxic for spinal motor neurons and their increased levels through disrupted tryptophan and lysine degradation may contribute to neuropathy.

In light of our findings, we have initiated a low lysine and tryptophan diet for the patient, which is used to treat glutaric aciduria type I (ref. 40) although so far without significant clinical benefit in the patient. Follow-up examinations of the patient will enable a better estimation of the efficacy of dietary interventions.

In summary, we combined a wide range of genetic, biochemical, molecular, metabolic, and bioinformatics techniques to pinpoint the pathomechanism resulting from a novel mitochondrial carrier protein deficiency. Each of these techniques were needed to support the molecular diagnosis, highlighted important targets, helped to better understand the

pathomechanism of disease in this patient, and also provided important insights for studies in other neurological and metabolic diseases.

SUPPLEMENTARY MATERIAL

Supplementary material is linked to the online version of the paper at http://www.nature.com/gim

AUTHOR CONTRIBUTIONS

V.B., M.S.K., A.C.S., F.E. and A.J.R. performed the experiments, analysed the data and participated in the drafting of the manuscript, B.B., V.R. and R.G.W. provided clinical information, A.R. and C.B. performed for the metabolic testing, M.L., A.P. and H.G. did the bioinformatics evaluation and segregation analysis, T.P., M.O. and R.W.T. provided data on the muscle biopsy, H.L. and P.F.C. participated in drafting and revision of the manuscript, E.R.S.K. and R.H. participated in the study design, data analysis and drafted and revised the manuscript.

ACKNOWLEDGMENTS

R.H. is a Wellcome Trust Investigator (109915/Z/15/Z), who receives support from the Wellcome Centre for Mitochondrial Research (203105/Z/16/Z), Medical Research Council (UK) (MR/N025431/1), the European Research Council (309548), the Wellcome Trust Pathfinder Scheme (201064/Z/16/Z), and the Newton Fund (UK/Turkey, MR/N027302/1). H.L. receives funding from the European Union Seventh Framework Programme (FP7/2007–2013) under grant agreement no. 305444 (RD-Connect) and 305121 (Neuromics). A.R. acknowledges the financial support by the Ministerium für Innovation, Wissenschaft und Forschung des Landes Nordrhein-Westfalen, the Senatsverwaltung für Wirtschaft, Technologie und Forschung des Landes Berlin, and the Bundesministerium für Bildung und Forschung. R.W.T. is supported by the Wellcome Centre for Mitochondrial Research (203105/Z/16/Z), the Medical Research Council Centre for Translational Research in Neuromuscular Disease, Mitochondrial Disease Patient Cohort (UK) (G0800674), the Lily Foundation, and the UK NHS Highly Specialised Service for Rare Mitochondrial Disorders of Adults and Children. This research was funded by the Medical Research Council through programme grant MC_U105663139 to M.S.K. and E.R.S.K. and MC_U105674181 to A.C.S., F.E., and A.J.R. R.H. and E.R.S.K. also gratefully acknowledge the Marie-Curie Initial Training Networks grant MEET (Mitochondrial European Educational Training Project, grant agreement 317433) for the collaboration.

DISCLOSURE

The authors declare no conflict of interest.

REFERENCES

1. Palmieri F. Mitochondrial transporters of the SLC25 family and associated diseases: a review. *J Inherit Metab Dis* 2014;37:565–575.
2. Shamseldin HE, Smith LL, Kentab A, et al. Mutation of the mitochondrial carrier SLC25A42 causes a novel form of mitochondrial myopathy in humans. *Hum Genet* 2016;135:21–30.
3. Abrams AJ, et al. Mutations in SLC25A46, encoding a UGO1-like protein, cause an optic atrophy spectrum disorder. *Nat Genet* 2015;47:926–932.
4. Wibom R, et al. AGC1 deficiency associated with global cerebral hypomyelination. *N Engl J Med* 2009;361:489–495.
5. Mayr JA, et al. Deficiency of the mitochondrial phosphate carrier presenting as myopathy and cardiomyopathy in a family with three affected children. *Neuromuscul Disord* 2011;21:803–808.
6. Fiermonte G, et al. Identification of the human mitochondrial oxodicarboxylate carrier. Bacterial expression, reconstitution, functional characterization, tissue distribution, and chromosomal location. *J Biol Chem* 2001;276:8225–8230.
7. Rehm HL, et al. ACMG clinical laboratory standards for next-generation sequencing. *Genet Med* 2013;15:733–747.
8. Olahova M, et al. LRPPRC mutations cause early-onset multisystem mitochondrial disease outside of the French-Canadian population. *Brain* 2015;138:3503–3519.
9. King MS, Boes C,, Kunji ER. Membrane protein expression in *Lactococcus lactis*. *Methods Enzymol* 2015;556:77–97.
10. Smith AC, Eyassu F, Mazat J-P, Robinson AJ. MitoCore: a curated constraint-based model for simulating human central metabolism. *BMC Syst Biol.* 2017:11(1);114.
11. Banos G, Daniel PM, Moorhouse SR, Pratt OE,, Wilson PA. The influx of amino acids into the heart of the rat. *J Physiol* 1978;280:471–486.
12. Becker SA, et al. Quantitative prediction of cellular metabolism with constraint-based models: the COBRA Toolbox. *Nat Protoc* 2007;2:727–738.
13. Han J, Gagnon S, Eckle T, Borchers CH. Metabolomic analysis of key central carbon metabolism carboxylic acids as their 3-nitrophenylhydrazones by UPLC/ESI-MS. *Electrophoresis* 2013;34:2891–2900.
14. Bartsakoulia M, et al. Cysteine supplementation may be beneficial in a subgroup of mitochondrial translation deficiencies. *J Neuromuscul Dis* 2016;3:363–379.
15. Blakely E, et al. Novel mutations in the TK2 gene associated with fatal mitochondrial DNA depletion myopathy. *Neuromuscul Disord* 2008;18:557–560.
16. King MS, Kerr M, Crichton PG, Springett R, Kunji ER. Formation of a cytoplasmic salt bridge network in the matrix state is a fundamental step in the transport mechanism of the mitochondrial ADP/ATP carrier. *Biochim Biophys Acta* 2016;1857:14–22.
17. Monne M, Chan KW, Slotboom DJ, Kunji ER. Functional expression of eukaryotic membrane proteins in *Lactococcus lactis*. *Protein Sci* 2005;14:3048–3056.
18. Cappello AR, et al. Functional and structural role of amino acid residues in the odd-numbered transmembrane alpha-helices of the bovine mitochondrial oxoglutarate carrier. *J Mol Biol* 2007;369:400–412.
19. Bansagi B, et al. Genetic heterogeneity of motor neuropathies. *Neurology* 2017;88:1226–1234.
20. Meyertholen K, Ravnan JB,, Matalon R. Identification of a novel 14q13.3 deletion involving the SLC25A21 gene associated with familial synpolydactyly. *Mol Syndromol* 2012;3:25–29.
21. Thompson K, et al. Recurrent de novo dominant mutations in SLC25A4 cause severe early-onset mitochondrial disease and loss of mitochondrial DNA copy number. *Am J Hum Genet* 2016;99:860–876.
22. Pebay-Peyroula E, et al. Structure of mitochondrial ADP/ATP carrier in complex with carboxyatractyloside. *Nature* 2003;426:39–44.
23. MacArthur DG, et al. Guidelines for investigating causality of sequence variants in human disease. *Nature* 2014;508:469–476.
24. Danhauser K, et al. DHTKD1 mutations cause 2-aminoadipic and 2-oxoadipic aciduria. *Am J Hum Genet* 2012;91:1082–1087.
25. Xu WY, et al. A nonsense mutation in DHTKD1 causes Charcot-Marie-Tooth disease type 2 in a large Chinese pedigree. *Am J Hum Genet* 2012;91:1088–1094.
26. Xu W, et al. DHTKD1 is essential for mitochondrial biogenesis and function maintenance. *FEBS Lett* 2013;587:3587–3592.
27. Govaerts L, Monnens L, Tegelaers W, Trijbels F,, van Raay-Selten A. Cerebro-hepato-renal syndrome of Zellweger: clinical symptoms and relevant laboratory findings in 16 patients. *Eur J Pediatr* 1982;139:125–128.
28. Tranchant C, et al. A new peroxisomal disease with impaired phytanic and pipecolic acid oxidation. *Neurology* 1993;43:2044–2048.
29. Kelley RI, Moser HW. Hyperpipecolic acidemia in neonatal adrenoleukodystrophy. *Am J Med Genet* 1984;19:791–795.
30. Tondo M, et al. Clinical, biochemical, molecular and therapeutic aspects of 2 new cases of 2-aminoadipic semialdehyde synthase deficiency. *Mol Genet Metab* 2013;110:231–236.

31. Dancis J, Hutzler J. The significance of hyperpipecolatemia in Zellweger syndrome. *Am J Hum Genet* 1986;38:707–711.
32. Houten SM, et al. Genetic basis of hyperlysinemia. *Orphanet J Rare Dis* 2013;8:57.
33. Braidy N, Grant R, Adams S, Brew BJ, Guillemin GJ. Mechanism for quinolinic acid cytotoxicity in human astrocytes and neurons. *Neurotox Res* 2009;16:77–86.
34. Chen Y, Brew BJ,, Guillemin GJ. Characterization of the kynurenine pathway in NSC-34 cell line: implications for amyotrophic lateral sclerosis. *J Neurochem* 2011;118:816–825.
35. Lugo-Huitron R, et al. Quinolinic acid: an endogenous neurotoxin with multiple targets. *Oxid Med Cell Longev* 2013;2013:104024.
36. Vamos E, Pardutz A, Klivenyi P, Toldi J,, Vecsei L. The role of kynurenines in disorders of the central nervous system: possibilities for neuroprotection. *J Neurol Sci* 2009;283:21–27.
37. Schwarcz R. The kynurenine pathway of tryptophan degradation as a drug target. *Curr Opin Pharmacol* 2004;4:12–17.
38. Brown GC. Regulation of mitochondrial respiration by nitric oxide inhibition of cytochrome c oxidase. *Biochim Biophys Acta* 2001;1504: 46–57.
39. Barker JE, Bolanos JP, Land JM, Clark JB, Heales SJ. Glutathione protects astrocytes from peroxynitrite-mediated mitochondrial damage: implications for neuronal/astrocytic trafficking and neurodegeneration. *Dev Neurosci* 1996;18:391–396.
40. Boy N, Haege G, Heringer J, et al. Low lysine diet in glutaric aciduria type I—effect on anthropometric and biochemical follow-up parameters. *J Inherit Metab Dis* 2013;36:525–533.
41. Arnold K, Bordoli L, Kopp J, Schwede T, et al. The SWISS-MODEL Workspace: A web-based environment for protein structure homology modelling. *Bioinformatics* 2006;22:195–201.